

Mechanical and Thermomechanical Elastic-Plastic Contact Analysis of Layered Media with Patterned Surfaces

Z.-Q. Gong, Graduate Student
K. Komvopoulos, Professor, Fellow ASME

Department of Mechanical Engineering
University of California
Berkeley, CA 94720

Abstract

An elastic-plastic finite element analysis of a sphere indenting and sliding over a layered medium with a patterned surface consisting of equally spaced rectangular pads was conducted in order to investigate the effect of the pattern geometry on the contact pressure distribution and subsurface stress-strain field. Three-dimensional sliding simulations were performed for lateral displacement of the indenting sphere approximately equal to two times the pad period. Three complete loading cycles, involving indentation, sliding, and unloading of a rigid sphere, were simulated to assess the effect of repeated sliding on the stresses in the first (hard) layer and plastic deformation in the underlying (soft) layer. Thermomechanical sliding contact simulations for an elastic-plastic layered medium with a patterned surface and an elastic-plastic sphere with properties identical to those of the first layer were carried out to examine the effect of frictional heating on the deformation behavior of the medium. Results are presented for the temperature distribution and maximum temperature variation at the surface and the evolution of subsurface plasticity in terms of Peclet number. The likelihood of thermal cracking in the wake of microcontacts during sliding is interpreted in the context of the thermal tensile stress caused by temperature gradients in the layered medium.

1. Introduction

Enhancement of the tribological performance and functionality of contacting surfaces is commonly achieved through deposition of thin surface layers (overcoats) exhibiting high hardness and low coefficient of friction. Analysis of the stresses and deformation in layered media due to sliding contact is critical to the design of many mechanical components. The primary objective in previous theoretical and numerical analyses has been the examination of the effect of the thickness and mechanical properties of protective overcoats on the contact stress and strain fields in the overcoat and underlying substrate media. However, relatively less is known about the role of surface geometry microfeatures (typically produced by lithography and electron beam techniques) on the elastic-plastic deformation and temperature rise due to frictional heating in layered media. Patterned layered media are used in many leading-edge technologies, such as high-density data storage (Chou et al., 1996; White et al., 1997) and magnetic random access memory media (Savas et al., 1999). Achromatic interferometric lithography has been used to fabricate arrays of microstructures with spatial periodicity of ~ 100 nm for ultra-high density magnetic storage applications (Farhoud et al., 1998; Savas et al., 1999).

Contact of elastic bodies possessing small-amplitude sinusoidal surfaces has been examined in early analytical studies in order to shed light into the effect of surface geometry on the contact stresses. Using complex variables, Westergaard (1939) obtained a closed form solution for the elastic contact of a sinusoidal surface and a smooth plane. Dundurs et al. (1973) used a Fourier analysis in a stress function approach to solve the previous problem. Johnson et al. (1985) determined the pressure distribution and contact area, and derived closed-form asymptotic solutions for both light and heavy contact loads resulting in almost full contact. Komvopoulos and Choi (1992) analyzed normal contact between regularly spaced rigid asperities and an elastic

half-space and obtained finite element solutions for the maximum contact pressure, normal load, and subsurface stresses in terms of the asperity distribution and indentation depth. Ramachandra and Ovaert (2000) examined the stresses produced in discontinuous coatings for different coating profiles and mechanical properties of the coating and substrate materials, and observed a significant decrease of the contact pressure peaks when the coating discontinuities possessed crowned edges. Gong and Komvopoulos (2003) analyzed normal and sliding contact of a rigid cylindrical asperity on patterned elastic-plastic layered media using the finite element method to reveal the effect of the pattern geometry on the resulting deformation and stress fields. While the maximum plastic strain due to sliding contact decreased with increasing amplitude-to-wavelength ratio of sinusoidal surface patterns, the high surface tensile stress at the trailing edge of the contact region indicated a greater probability of surface cracking for patterned media.

The temperature rise at sliding interfaces due to frictional heating may affect significantly the tribological behavior of electromechanical components. Thermomechanical analysis of homogeneous half-spaces subjected to a fast moving heat source have shown that the surface stress field is predominantly compressive (Ju and Huang, 1982), and the maximum thermal tensile stress occurs slightly below the trailing edge of the contact region (Huang and Ju, 1985) at a depth where the temperature gradient begins to vanish (Ju and Liu, 1988). This critical depth depends on the Peclet number, which is a function of sliding speed, contact radius, and material diffusivity. Ju and Chen (1984) conducted a thermomechanical contact analysis for layered media under a moving friction load and a moving heat source and discussed crack initiation based on the determined stress field. Leroy et al. (1989) derived a two-dimensional model for a layered medium subjected to a translating heat source and reported high stresses in overcoats with thermomechanical properties significantly different from those of the substrate material.

Cho and Komvopoulos (1997) performed a fracture mechanics analysis of subsurface crack propagation and showed that, while frictional heating exhibits a negligible effect on the crack propagation direction, it increases the in-plane crack growth rate and reduces the critical crack length at the onset of out-of-plane growth at the right crack tip. In a more recent study, Ye and Komvopoulos (2003) developed a finite element model to examine the simultaneous effects of mechanical and thermal surface traction on the deformation of elastic-plastic layered media, and interpreted the propensity for plastic flow and cracking in terms of the thickness and thermal properties of the layer, normal load, and Peclet number.

Despite important insight into thermomechanical contact deformation of elastic-plastic media derived from previous studies, a comprehensive three-dimensional contact analysis for elastic-plastic patterned layered media has not been reported yet. Therefore, the principal objective of this study was to examine the effects of pattern geometry, coefficient of friction, indenter sharpness (radius), and sliding cycles on the stresses and strains arising in layered patterned media subjected to normal and shear (friction) surface tractions. Another objective was to analyze the effect of frictional heating on the surface temperature distribution and subsurface plasticity. Deformation and frictional heating in patterned layered media is discussed in the context of finite element results for the contact pressure distribution, subsurface stress/strain fields, and temperature rise at the contact surface obtained for different indentation depths, coefficient of friction, sliding cycles, indenter radius, and Peclet number.

2. Modeling Procedures

2.1 Finite Element Model

Figure 1 shows a three-dimensional finite element model of a sphere in contact with an elastic-plastic layered medium with a patterned surface. Due to symmetry, only one-half of the

sphere and layered medium were modeled in order to reduce the computation time. The finite element mesh consists of 25,732 eight-node linear interpolation elements having a total of 33,099 nodes. The normalized mesh dimensions are $x/H = 2.443$, $y/H = 0.260$, and $z/H = 1.0$, where H is the total thickness of the mesh. Four pads of constant height of $0.86b$ and equally spaced at lateral distances $l = 0.714b$, where b is the side of the square pad surfaces, were modeled at the surface of the finite element mesh (i.e., pad period equal to $b + l$). In these simulations, the sphere was assumed to be rigid with a radius of curvature $R/H = 0.763$ and 1.526 . Sliding was simulated by displacing the sphere along the positive x -direction in an incremental fashion. The nodes on planes $x = 0$, $y = 0$, and $z = 0$ were constrained against displacement in the x -, y -, and z -direction, respectively. In the thermomechanical analysis, the length of the finite element mesh was reduced to $x/H = 1.588$ and the number of pads to three due to the excessive computation time in coupled thermal and mechanical contact analysis. Therefore, the mesh in the thermomechanical simulations consisted of 20,995 eight-node, coupled temperature-displacement finite elements comprising a total of 27,585 nodes. In addition, the sphere was assumed to be elastic-perfectly plastic with a radius of curvature $R/H = 1.526$ and thermomechanical properties identical to those of the first layer. The temperature at the nodes of planes $y = 0$, and $x/H = 0$ and 1.588 was set equal to $20\text{ }^{\circ}\text{C}$. Heat conduction was restricted across the sphere/layered medium contact interface.

2.2 Material Properties and Constitutive Models

The normalized thickness, h/H , and elastic-plastic properties of each layer material of the patterned layered medium are given in Table 1. These thickness and mechanical property values are typical of layers used in magnetic recording rigid disks consisting of carbon overcoat (layer 1), CoCrPt magnetic medium (layer 2), and CrV underlayer (layer 3) deposited on NiP-coated

Al-Mg substrate. The elastic modulus and yield strength of layers 1 and 2 have been determined from nanoindentation measurements (Komvopoulos, 2000). The specific heat, thermal conductivity, and density of the first layer are representative of carbon films (Graebner, 1996; Morath et al., 1994; Tsai and Bogy, 1987). All other density and thermal properties were obtained from data compiled by Kaye and Laby (1986).

Yielding at a material point occurred when the von Mises equivalent stress, σ_M , satisfied the yield condition,

$$\sigma_M = \left[\frac{3}{2} S_{ij} S_{ij} \right]^{1/2} = \sigma_Y, \quad (1)$$

where S_{ij} denotes the components of the deviatoric stress tensor, and σ_Y is the tensile yield strength under uniaxial tension. Plastic deformation was based on the usual associated flow rule, assuming negligible plastic volume change. To account for nonlinearities, an updated Lagrangian formulation was used in all the simulations. Each layer was modeled as an elastic-perfectly plastic material. The equivalent plastic strain, $\bar{\epsilon}_p$, defined as

$$\bar{\epsilon}_p = \int_{\Gamma} \sqrt{\frac{2}{3} d\mathbf{e}_{ij}^p d\mathbf{e}_{ij}^p}, \quad (2)$$

where \mathbf{G} is the strain path, was used to track the evolution of plasticity in the layered medium. The usual elastic constitutive equations were used when $\sigma_M < \sigma_Y$, and the plastic flow rule was applied at material points where the von Mises yield condition $\sigma_M = \sigma_Y$ was satisfied.

2.3 Thermal Model

Sliding friction at contact interfaces of mechanical components promotes dissipation of energy in the form of heat within the vicinity of the real contact area. The dissipated frictional heat is responsible for the temperature rise at the contact interface of sliding bodies, causing the

development of thermal stresses and variations in the real contact area and contact pressure distribution due to thermal expansion. Since these changes in the contact conditions affect the heat generation rate and heat conduction across the contact interface, the thermal and mechanical stress/strain fields are fully coupled and, therefore, must be determined simultaneously rather than sequentially. In this study, the temperature was integrated based on a backward-difference scheme, and the coupled system was solved using the Newton method. A fully coupled thermal-stress analysis automatically invokes a nonsymmetric matrix storage and solution scheme to improve the computational efficiency. This is because the stiffness matrix is asymmetric due to friction and the convective term in the conduction-convection equation.

The heat flux density due to frictional heat, q , is given by

$$q = hmpu , \quad (3)$$

where h is the fraction of mechanical work dissipated as heat, m is the coefficient of friction, p is the contact pressure, and u is the sliding speed. In the present simulations, it is assumed that $h = 1.0$, which is consistent with the conclusion of Uetz and Föhl (1978) that nearly all the energy dissipated in a frictional contact is transformed into heat. The amount of frictional heat instantaneously conducted into each contacting body depends on the heat partition factor.

Although the contact interface was modeled to have zero heat capacity, it was assigned properties for the exchange of heat by conduction and radiation, as in a previous study (Ye and Komvopoulos, 2003). However, heat flux due to radiation was neglected as much smaller than that due to conduction. The flux density across the contact interface (from the sphere to the layered medium), q_c , is defined as

$$q_c = k_g (\mathbf{q}_1 - \mathbf{q}_2) , \quad (4)$$

where q_1 and q_2 are temperatures at surface nodes of the contacting bodies (i.e., the sphere and patterned layered medium, respectively), and k_g is the gap conductance, defined as k/Dl , where k is the thermal conductivity of the first layer, and Dl is the size of the smallest finite element.

The heat flux density into each contacting body, q_1 and q_2 , respectively, is given by

$$\begin{aligned} q_1 &= -q_c + fq \\ q_2 &= q_c + (1-f)q \end{aligned} \quad (5)$$

where f is the heat partition factor indicating the fraction of heat dissipated into one of the contacting bodies (sphere). Simulations were performed for $f = 0.5$, i.e., evenly distributed heat between the sphere and the layered medium.

2.4 Finite Element Simulations

Quasi-static contact simulations comprising three sequential steps of loading, sliding, and unloading of a sphere on a layered patterned medium were performed in an incremental fashion. Normal contact (indentation) was simulated by advancing the sphere toward the elastic-plastic medium up to a specified indentation depth, d (or normal load). Subsequently, the sphere was displaced laterally to a maximum distance, S , of about ten times the contact radius maintaining constant indentation depth d and coefficient of friction, m and then unloaded following the same steps as for the loading. All simulations were performed with the multipurpose finite element code ABAQUS. Friction coefficient values of 0.1 and 0.5 were used in the simulations in order to study the effect of friction on the stress/strain fields produced in the layered medium. In addition, consecutive passes of the sphere were simulated to investigate the dependence of stress and plastic strain on sliding cycles. The thermomechanical simulations were performed for $m = 0.5$ and Peclet number $Pe = 2ur/a$, where r is the contact radius after indentation, and a is the thermal diffusivity of the sphere, equal to 0.09 and 0.9.

3. Results and Discussion

Finite element solutions for the stresses and strains in an elastic-plastic layered medium due to indentation and sliding of a rigid sphere are presented first in order to elucidate the significance of surface microgeometry (patterning) on contact deformation and to establish a reference for comparison with thermomechanical analysis results. The effects of friction coefficient, sphere radius, and sliding cycles are discussed next in terms of results for the contact pressure, contact area, subsurface stresses, and maximum plastic strain. Lastly, simulation results from a fully coupled thermomechanical contact analysis of an elastic-plastic sphere indenting and sliding over an elastic-plastic layered patterned medium are presented to illustrate the effect of frictional heating on the surface temperature rise and subsurface deformation.

3.1 Contact Mechanics Analysis

Figure 2 shows the contact pressure distribution (in the plane of symmetry $y = 0$) produced on a single pad due to indentation by a rigid sphere versus normalized indentation depth, d/R . Initial contact occurred at the center of the pad ($x/b = 0$). For shallow indentations ($d/R = 0.0025$), the contact pressure distribution is similar to the profile predicted by the Hertz theory. However, increasing the indentation depth ($d/R = 0.005$ and 0.0075) causes the maximum contact pressure to shift from the center to the edge of the contact area (Fig. 2(a)). Further increase of the indentation depth ($d/R \geq 0.01$) produces pressure spikes at the edges of the contact area (Fig. 2(b)), consistent with the contact pressure profile obtained for a layered medium with a meandered surface pattern (Gong and Komvopoulos, 2003). This change of the contact pressure is attributed to the development of a plastic zone in the second soft layer and the relatively higher rigidity of the pad sides. The asymmetry of the contact pressure profiles at large indentation depths (i.e., $d/R = 0.0125$ and 0.015) is due to the constraint of the nodes on plane

$x/H = 0$ against displacement in the x -direction. However, this effect was negligible in the results presented below due to the much smaller indentation depth used in these simulations. The normalized maximum von Mises equivalent stress in the first layer, $\mathbf{s}_M^{\max} / \mathbf{s}_{Y1}$, and normalized real contact area, A_r / A_p , are plotted in Figs. 3(a) and 3(b), respectively, as functions of normalized indentation depth, d/R , where \mathbf{s}_{Y1} is the yield strength of the first layer and A_p is the pad surface area. For relatively shallow indentations (i.e., partial contact between the sphere and the pad surface), both maximum Mises stress and contact area increase monotonically with indentation depth. For $d/R > 0.008$, the maximum Mises stress reaches the yield strength of the layer material and a small plastic zone develops adjacent to the contact interface. Full contact of the pad with the sphere occurs when $d/R \geq 0.1$. Thus, elastic and elastic-plastic deformation of the pad is associated with partial and full contact with the sphere, respectively.

The variation of the maximum contact pressure, p_{\max} , and maximum equivalent plastic strain in the second layer, $\bar{\mathbf{e}}_p^{\max}$, with normalized sliding distance, S/R , for $\mathbf{m} = 0.1$ and 0.5 is shown in Figs. 4(a) and 4(b), respectively. The periodic fluctuation of the maximum contact pressure is due to the pattern geometry. The fact that the two peak values of p_{\max} are fairly close suggests that interaction between neighboring pads is secondary. The $\bar{\mathbf{e}}_p^{\max}$ strain in the second layer increases significantly at the beginning of sliding, reaching a steady state at a distance of about two times the pad period ($S/R = 0.48$). However, a longer sliding distance for the plastic strain to reach a steady state was found for a layered medium with a smooth (flat) surface (Gong and Komvopoulos, 2003). This major difference between patterned and smooth layered media is due to the reduced plastic deformation in the patterned medium. As shown in Figs. 4(a) and 4(b), the coefficient of friction influences profoundly both the maximum contact pressure and the plastic

strain in the second layer. Although the pressure and strain results for $m = 0.1$ and 0.5 exhibit similar trends, much higher peak values of contact pressure and plastic strain were obtained with the higher coefficient of friction

Figure 5 shows the evolution of the equivalent plastic strain in the layered medium with sliding distance for $m = 0.5$ and $d/R = 0.005$. For pure normal contact ($S/R = 0$, Fig. 5(a)), the maximum plastic strain occurs below the contact interface and the plastic zone is confined in the second layer. Sliding of the sphere over the pad edge ($S/R = 0.07$, Fig. 5(b)) causes the formation of two small plastic zones in the second layer at the lower right corner of the pad due to the effect of stress concentration. When the sphere slides over the next pad ($S/R = 0.12$, Fig. 5(c)), stress concentration produces a small plastic zone in the first layer at the upper left corner of this pad, and the maximum plastic strain occurs at the interface of the two layers, similar to smooth layered media (Kral and Komvopoulos, 1997). Figures 5(d)-5(f) show that the maximum equivalent plastic strain occurs always at the interface of the first and second layers. The close similarity of the plastic zones in each pad confirms that interaction of the stress fields in each pad is negligible and that deformation depends only on the pad geometry and mechanical properties of each layer material.

The dependence of the maximum von Mises equivalent stress in the first layer and maximum equivalent plastic strain in the second layer on the distance and cycles of sliding is shown in Fig. 6 for $m = 0.1$ and $d/R = 0.005$. The close agreement between the results of the second and third sliding cycles suggests that, for the simulated friction coefficient and indentation depth, a steady-state stress/strain field is reached after two sliding cycles. The change of \mathbf{s}_M^{\max} after the first sliding cycle (Fig. 6(a)) is a consequence of the residual stress due to the permanent distortion of the pads in the first sliding cycle. The peak value of $\bar{\mathbf{e}}_p^{\max}$ is reached

during the first sliding cycle and does not change with additional sliding cycles (Fig. 6(b)). This behavior differs from that of a layered medium with a smooth surface for which, $\bar{\epsilon}_p^{\max}$ increases with sliding cycles (Kral and Komvopoulos, 1996). In addition, the peak value of $\bar{\epsilon}_p^{\max}$ in the patterned medium is equal to ~ 0.036 , which is significantly less than that of the smooth layered medium (Gong and Komvopoulos, 2003). The appreciably less plastic deformation and insignificant effect of repetitive sliding on the stress and strain fields of patterned layered media (compared to smooth layered media) demonstrates the beneficial effect of surface patterning in sliding contact deformation.

The effect of the sharpness of the rigid spherical indenter on the normalized \mathbf{s}_M^{\max} in the first layer and $\bar{\epsilon}_p^{\max}$ in the second layer can be analyzed by comparing the results for $d/R = 0.005$ and 0.01 shown in Fig. 7. The sliding distance S is normalized by the pad period, $b + l$. As mentioned in the discussion of Fig. 6(a), the periodic fluctuation of \mathbf{s}_M^{\max} with sliding distance (Fig. 7(a)) is due to the pattern geometry. Significantly larger values of \mathbf{s}_M^{\max} in the first (hard) layer (Fig. 7(a)) and $\bar{\epsilon}_p^{\max}$ in the second (soft) layer (Fig. 7(b)) are produced with the relatively sharp sphere. The Mises yield condition in the hard layer ($\mathbf{s}_M^{\max}/\mathbf{s}_{Y1} = 1.0$) is satisfied only in the case of the sharp sphere ($d/R = 0.01$). A steady-state $\bar{\epsilon}_p^{\max}$ is obtained in the soft layer after the sphere slides a distance of about two times the pad period, for both $d/R = 0.005$ and 0.01 . The results shown in Fig. 7 illustrate the dependence of plasticity in hard overcoats on the indenter sharpness. Thus, small plastic zones may be produced even in ultrathin surface layers under relatively light contact loads, depending on the range of small wavelengths comprising the surface profile.

3.2 Thermomechanical Analysis

Finite element results from a fully-coupled thermomechanical contact analysis of an elastic-perfectly plastic sphere (with thermomechanical properties identical to those of the first layer) sliding over the patterned medium are presented in Figs. 8-10 to illustrate the effect of frictional heating on the surface temperature rise and plastic flow in the soft layer. Temperature and plastic strain results are interpreted in terms of sliding distance and Peclet number. To examine the effect of Peclet number on the temperature field and deformation behavior of the layered medium, simulation results are presented for $m = 0.5$ and $Pe = 0.09$ and 0.9 .

Figure 8 shows the evolution of the surface temperature distribution on three neighboring pads along the plane of symmetry ($y = 0$) for $Pe = 0.09$ and $d/R = 0.01$. The results are presented as a temperature increase from the room temperature, ΔT , normalized by $2\bar{q}a/pku$, where \bar{q} is the average heat flux rate at the contact region (i.e., total heat flux divided by the contact area, πr^2), and k is the thermal conductivity of the sphere, while the x coordinate is normalized by the contact radius, r . As expected, the temperature distribution due to normal contact (indentation) of a single pad is symmetric and its effect on neighboring pads is negligible (Fig. 8(a)). When the sphere slides over the edge of the left pad (Fig. 8(b)), the maximum temperature increases significantly and shifts to the trailing edge of the contact region (Fig. 8(b)), demonstrating a pronounced effect of frictional heating during sliding. The maximum temperature rise at the trailing edge produces a maximum tensile thermal stress slightly below this contact edge, which is considered to be responsible for thermal cracking in the wake of sliding microcontacts. In addition, a noticeable temperature rise occurs at the front contact edge as soon as the sphere establishes contact with the middle pad. This temperature rise intensifies significantly when the

sphere slides over the left corner of the middle pad (Fig. 8(c)), evidently due to the high pressure peak at the sharp corner of the pad edge. A similar temperature evolution is observed as the sphere slides over the middle and right pads (Figs. 8(d)-8(f)). The close similarity of the temperature distributions produced when the sphere is over the center of the middle and right pads (Figs. 8(d) and 8(f)) suggests that frictional heating at a pad is not affected by the heat flux at neighboring pads.

Figures 9(a) and 9(b) show the normalized maximum temperature, T_{\max} , in the first and second layers, respectively, as functions of normalized sliding distance and Peclet number. The maximum temperature in the first layer occurs at the surface and in the second layer at the interface with the first layer. The periodic fluctuation of T_{\max} with sliding distance observed only for $Pe = 0.9$ suggests that the pattern geometry effect on the maximum temperature in each layer is pronounced only for a relatively high Peclet number. The marked increase of T_{\max} in both layers obtained for $Pe = 0.9$, especially at the surface of the first layer (Fig. 9(a)), demonstrates that the temperature field in the layered medium is a strong function of the Peclet number. The similar peak values of T_{\max} in Fig. 9(a) indicate that interaction between neighboring pads is negligible. Furthermore, comparison of the results shown in Figs. 9(a) and 9(b) for $Pe = 0.9$ shows that values of T_{\max} in the first layer are much higher than those in the second layer. In the sliding simulations for $m = 0.5$ and $Pe = 0.9$, the highest temperature change in the first and second layers was found to be equal to ~ 220 °C and ~ 50 °C, respectively. Such high surface temperatures may induce thermal cracking and degrade the mechanical properties of the surface layer.

Figure 10 shows the variation of the maximum equivalent plastic strain in the second (soft) layer with normalized sliding distance and Peclet number for $m = 0.5$ and $d/R = 0.01$. A rapid

increase of $\bar{\epsilon}_p^{\max}$ at the beginning of sliding and a steady state at a sliding distance $S/R = 0.17$ is shown for both Peclet numbers. While the effect of the Peclet number on $\bar{\epsilon}_p^{\max}$ is negligible during the initial stage of sliding, larger values of $\bar{\epsilon}_p^{\max}$ (~5.7%) were produced with the higher Peclet number when $S/R > 0.17$. This is attributed to the fact that the surface temperature and difference between the maximum surface temperatures for $Pe = 0.09$ and 0.9 increase with sliding distance until $S/R > 0.17$ (Fig. 9(a)). This temperature difference produces a thermal stress that affects the plastic strain in the second layer. Thus, a higher Peclet number induces larger temperature rises at the surface of the first hard layer and larger plastic strains in the second soft layer of the medium.

4. Conclusions

A elastic-plastic finite element analysis of normal contact (indentation) and sliding of a spherical indenter on a layered medium with a patterned surface was performed in order to study the effects of coefficient of friction, sphere radius, and sliding cycles on the contact stress and deformation fields. In addition, a fully coupled thermomechanical finite element analysis was carried out to obtain solutions for the surface temperature distribution and to elucidate the effect of Peclet number on the maximum temperature rise and subsurface plasticity. Based on the presented results and discussion, the following main conclusions can be drawn.

1. The maximum contact pressure shifts from the center to the edge of the contact area at a critical indentation depth ($d/R > 0.005$). Pressure spikes occur at the contact edges in the case of relatively deep indentations ($d/R > 0.01$). For shallow indentations ($d/R < 0.01$), the maximum von Mises equivalent stress in the first layer and contact area increase monotonically with indentation depth. Yielding in the first (hard) layer adjacent to the

surface commences when $d/R > 0.008$, and full contact of a pad with the sphere occurs $d/R > 0.01$ when the sphere center is over the center of the pad surface.

2. The contact pressure and subsurface stresses and plastic strains exhibit periodic fluctuations due to the pattern geometry. The similarity of the stress/strain results of neighboring pads suggests that interaction effects are negligible for the modeled pattern geometry. High-friction sliding (i.e., $m = 0.5$) increases significantly the maximum equivalent plastic strain in the second (soft) layer during the beginning of sliding, leading to a steady state after a sliding distance about two times the pad period. The reduced plasticity in the soft layer of patterned layered media compared to that of smooth layered media demonstrates the beneficial effect of surface patterning in sliding contact.
3. Steady-state stress/strain fields were produced after the first sliding cycle, suggesting that deformation in the layered medium is independent of sliding cycles. This is a profound difference with smooth layered media, for which the maximum von Mises equivalent stress in the first layer and maximum equivalent plastic strain in the second layer have been found to increase significantly with sliding cycles. In low-friction sliding, relatively sharp spherical indenters promote the formation of small plastic zones in the first hard layer at the sharp corners of the pad edges.
4. Normal contact (indentation) of a pad yields a symmetric temperature distribution and negligible temperature rise at neighboring pads. Sliding intensifies the temperature field, causing the maximum temperature to shift from the center to the trailing edge of the contact region. This leads to the development of a high thermal tensile stress slightly below the trailing edge of the contact region, which is considered to be responsible for thermal cracking in the wake of sliding microcontacts.

5. The periodic variation of the maximum temperature rise in both the first and the second layer with sliding distance is due to the pattern geometry. The temperature field in the layered medium is a strong function of the Peclet number. The similar peak values of the maximum temperature in each layer illustrate that thermal interaction between neighboring pads is negligible. Increasing the Peclet number enhances the temperature rise at the surface and the development of thermal stresses in the first (hard) layer and produces larger plastic strains in the second (soft) layer and in small regions of the first layer, in the vicinity of the sharp pad edges.

Acknowledgments

This work was partially supported by the National Storage Industry Consortium (NSIC), Extremely-High Density Recording (EHDR) Program, and the Computer Mechanics Laboratory at the University of California at Berkeley.

References

Cho, S.-S., and Komvopoulos, K., 1997, "Thermoelastic Finite Element Analysis of Subsurface Cracking Due to Sliding Surface Traction," *ASME Journal of Engineering Materials and Technology*, **119**, pp.71-78.

Chou, S. Y., Krauss, P. R., and Kong, L., 1996, "Nanolithographically Defined Magnetic Structures and Quantum Magnetic Disk," *J. Appl. Phys.*, **79**, pp. 6101-6106.

Dundurs, J., Tsai, K. C., and Keer, L. M., 1973, "Contact of Elastic Bodies with Wavy Surfaces," *J. Elasticity*, **3**, pp. 109-115.

Farhoud, M., Hwang, M., Smith, H. I., Schattenburg, M. L., Bae, J. M., Youcef-Toumi, K., and Ross, C. A., 1998, "Fabrication of Large Area Nanostructured Magnets by Interferometric Lithography," *IEEE Trans. Mag.*, **34**, pp. 1087-1089.

- Gong, Z.-Q., and Komvopoulos, K., 2003, "Effect of Surface Patterning on Contact Deformation of Elastic-Plastic Layered Media," *ASME Journal of Tribology*, **125**, pp. 16-24.
- Graebner, J. E., 1996, "Measurements of Specific Heat and Mass Density in CVD Diamond," *Diam. Relat. Mater.*, **5**, pp. 1366-1370.
- Huang, J. H., and Ju, F. D., 1985, "Thermomechanical Cracking Due to Moving Frictional Loads," *Wear*, **102**, pp. 81-104.
- Johnson, K. L., Greenwood, J. A., and Higginson, J. G., 1985, "The Contact of Elastic Wavy Surfaces," *Int. J. Mech. Sci.*, **27**, pp. 383-396.
- Ju, F. D., and Huang, J. H., 1982, "Heat Checking in the Contact Zone of a Bearing Seal (A Two-Dimensional Model of a Single Moving Asperity)," *Wear*, **79**, pp. 107-118.
- Ju, F. D., and Chen, T. Y., 1984, "Thermomechanical Cracking in Layered Media from Moving Friction Load," *AMSE Journal of Tribology*, **106**, pp. 513-518.
- Ju, F. D., and Liu, J. C., 1988, "Effect of Peclet Number in Thermo-Mechanical Cracking Due to High-Speed Friction Load," *ASME Journal of Tribology*, **110**, pp. 217-221.
- Kaye, G. W. C., and Laby, T. H., 1986, *Tables of Physical and Chemical Constants and Some Mathematical Functions*, Longman, London, UK.
- Komvopoulos, K., 2000, "Head-Disk Interface Contact Mechanics for Ultrahigh Density Magnetic Recording," *Wear*, **238**, pp. 1-11.
- Komvopoulos, K., and Choi, D.-H., 1992, "Elastic Finite Element Analysis of Multi-Asperity Contacts," *ASME Journal of Tribology*, **114**, pp. 823-831.
- Kral, E. R., and Komvopoulos, K., 1996, "Three-Dimensional Finite Element Analysis of Subsurface Stresses and Shakedown Due to Repeated Sliding on a Layered Medium," *ASME J. Appl. Mech.*, **63**, pp. 967-973.

Kral, E. R., and Komvopoulos, K., 1997 “Three-Dimensional Finite Element Analysis of Subsurface Stresses and Strain Fields Due to Sliding Contact on an Elastic-Plastic Layered Medium,” ASME Journal of Tribology, **119**, pp. 332-341.

Leroy, J. M., Floquet, A., and Villechaise, B., 1989, “Thermomechanical Behavior of Multilayered Media: Theory,” ASME Journal of Tribology, **111**, pp. 538-544.

Morath, C. J., Maris, H. J., Cuomo, J. J., Pappas, D. L., Grill, A., Patel, V. V., Doyle, J. P., and Saenger, K. L., 1994, “Picosecond Optical Studies of Amorphous Diamond and Diamondlike Carbon: Thermal Conductivity and Longitudinal Sound Velocity,” J. Appl. Phys., **76**, pp. 2636-2640.

Ramachandra, S., and Ovaert, T. C., 2000, “Effect of Coating Geometry on Contact Stresses in Two-Dimensional Discontinuous Coatings,” ASME Journal of Tribology, **122**, pp. 665-671.

Savas, T. A., Farhoud, M., Smith, H. I., Hwang, M., and Ross, C. A., 1999, “Properties of Large-Area Nanomagnet Arrays with 100 nm Period Made by Interferometric Lithography,” J. Appl. Phys., **85**, pp. 6160-6162.

Tsai, H.-C., and Bogy, D. B., 1987, “Critical Review: Characterization of Diamondlike Carbon Films and Their Application as Overcoats on Thin-Film Media for Magnetic Recording,” J. Vac. Sci. Technol. A, **5**, pp. 3287-3312.

Uetz, H., and Föhl, J., 1978, “Wear as an Energy Transformation Process,” Wear, **49**, pp. 253-264.

Westergaard, H. M., 1939, “Bearing Pressures and Cracks,” ASME J. Appl. Mech., **6**, pp. 49-53.

White, R. L., New, R. M. H., and Pease, R. F. W., 1997, “Patterned Media: A Viable Route to 50 Gbit/in² and Up for Magnetic Recording,” IEEE Trans. Mag., **33**, pp. 990-995.

Ye, N., and Komvopoulos, K., 2003, “Three-Dimensional Finite Element Analysis of Elastic-Plastic Layered Media Under Thermomechanical Surface Loading,” ASME Journal of Tribology, **125**, pp. 52-59.

Table 1. Thickness and thermomechanical properties of layers in the patterned layered medium

Medium	Layer 1	Layer 2	Layer 3
Thickness (h/H)	0.015	0.374	0.611
Elastic modulus (GPa)	168	130	140
Poisson's ratio	0.3	0.3	0.3
Yield strength (GPa)	13	2.67	2.58
Thermal expansion (K^{-1})	3.1×10^{-6}	13×10^{-6}	4.9×10^{-6}
Specific heat (J/g K)	0.5	0.411	0.438
Conductivity (W/mK)	5.2	105	96.5
Density (kg/m^3)	2.15×10^3	8.9×10^3	7.19×10^3
Diffusivity (m^2/s)	4.84×10^{-6}	28.7×10^{-6}	30.64×10^{-6}

List of Figures

- Fig. 1. Three-dimensional finite element mesh of a layered medium with a patterned surface.
- Fig. 2. Contact pressure distribution on a single pad at the symmetry plane ($y = 0$) for different indentation depths. (Initial contact with the indenting rigid sphere occurs at the center of the pad surface ($x/b = 0$)).
- Fig. 3. (a) Maximum von Mises equivalent stress in the first (hard) layer and (b) real contact area versus indentation depth.
- Fig. 4. (a) Maximum contact pressure and (b) maximum equivalent plastic strain in the second (soft) layer versus sliding distance for $m = 0.1$ and 0.5 and $d/R = 0.005$.
- Fig. 5. Contours of equivalent plastic strain in the layered medium for $m = 0.5$, $d/R = 0.005$, and S/R equal to (a) 0, (b) 0.07, (c) 0.12, (d) 0.17, (e) 0.24, and (f) 0.48. (The arrow indicates the direction of the sliding rigid sphere.)
- Fig. 6. (a) Maximum von Mises equivalent stress in the first (hard) layer and (b) maximum equivalent plastic strain in the second (soft) layer versus sliding distance and sliding cycles for $m = 0.1$ and $d/R = 0.005$.
- Fig. 7. (a) Maximum von Mises equivalent stress in the first (hard) layer and (b) maximum equivalent plastic strain in the second (soft) layer versus sliding distance for $m = 0.1$ and $d/R = 0.005$ and 0.01 .
- Fig. 8. Surface temperature increase on individual pads along the plane of symmetry $y = 0$ for $m = 0.5$, $d/R = 0.01$, $Pe = 0.09$, and S/R equal to (a) 0, (b) 0.07, (c) 0.17, (d) 0.24, (e) 0.31, and (f) 0.48.
- Fig. 9. Maximum temperature in (a) first (hard) layer and (b) second (soft) layer versus sliding distance and Peclet number for $m = 0.5$ and $d/R = 0.01$.

Fig. 10 Maximum equivalent plastic strain in the second (soft) layer versus sliding distance and Peclet number for $m=0.5$ and $d/R=0.01$.

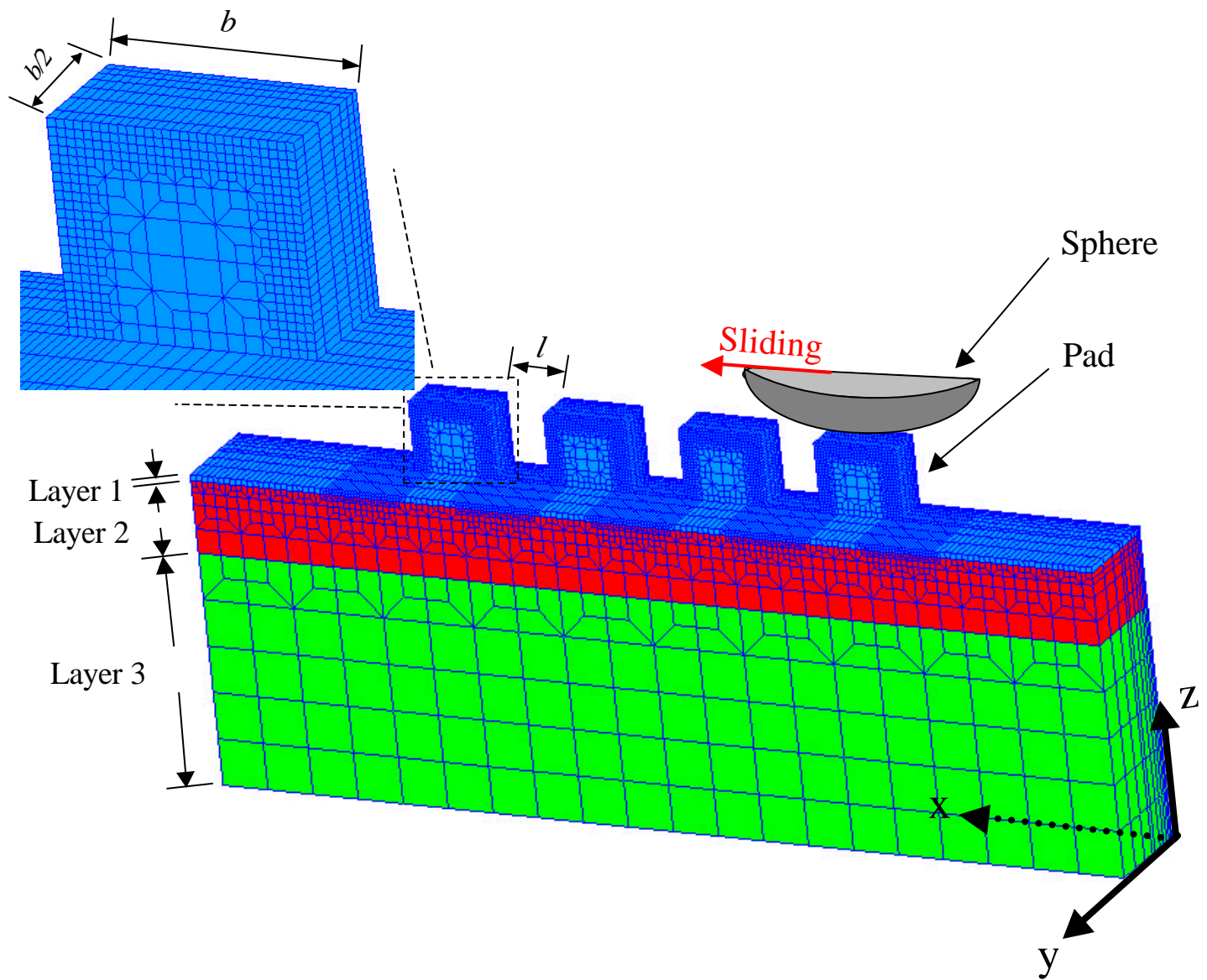


Figure 1

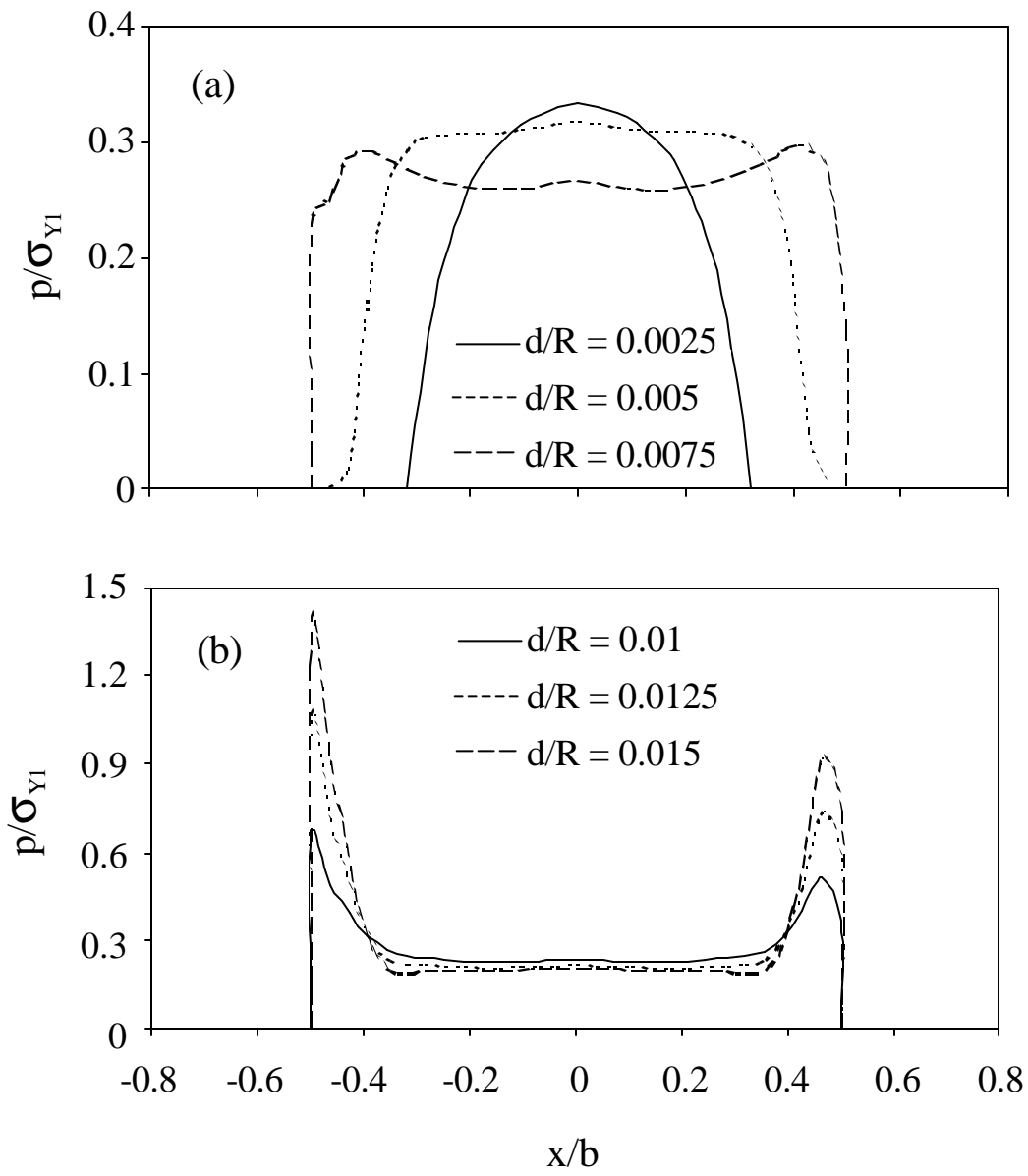


Figure 2

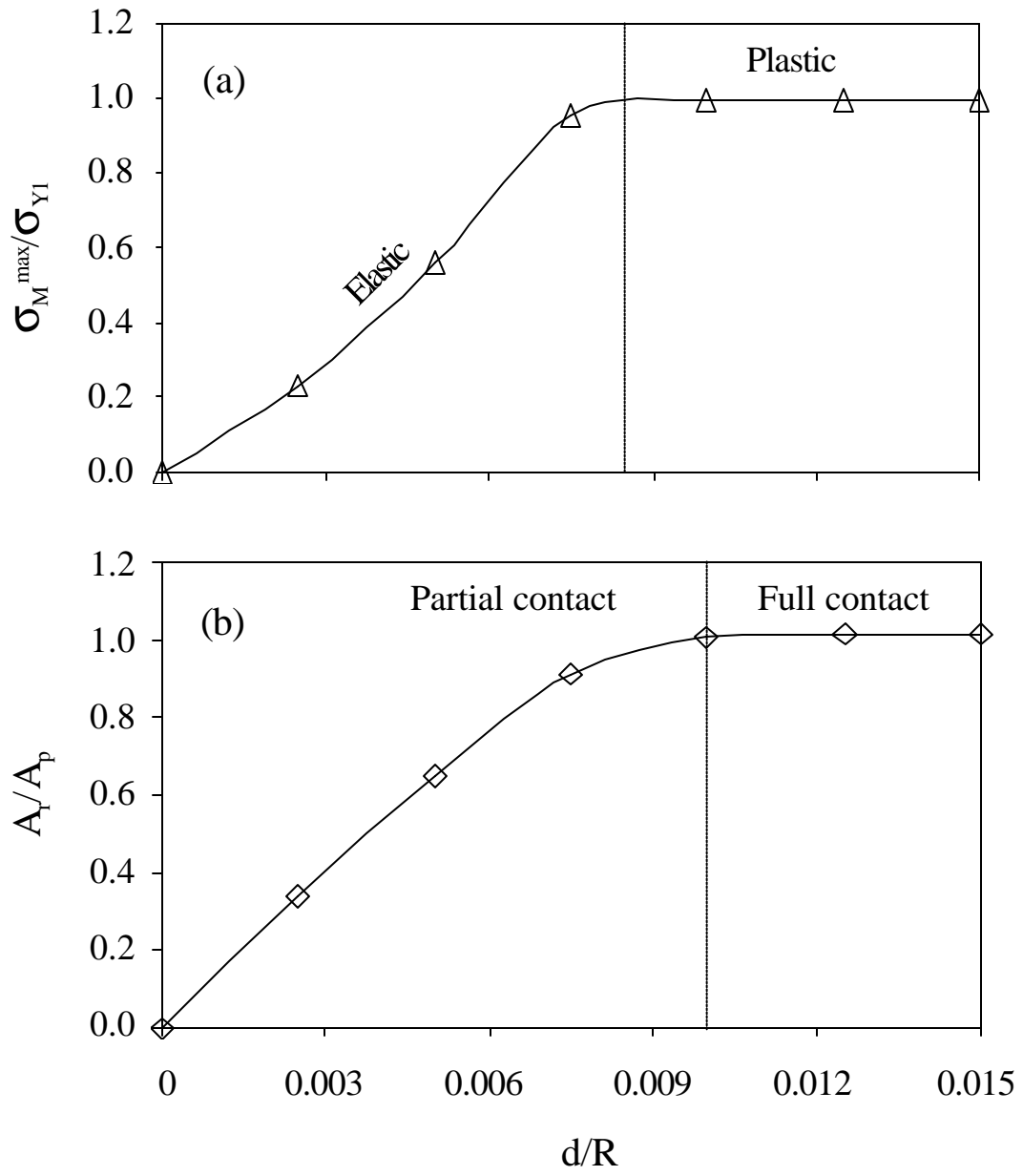


Figure 3

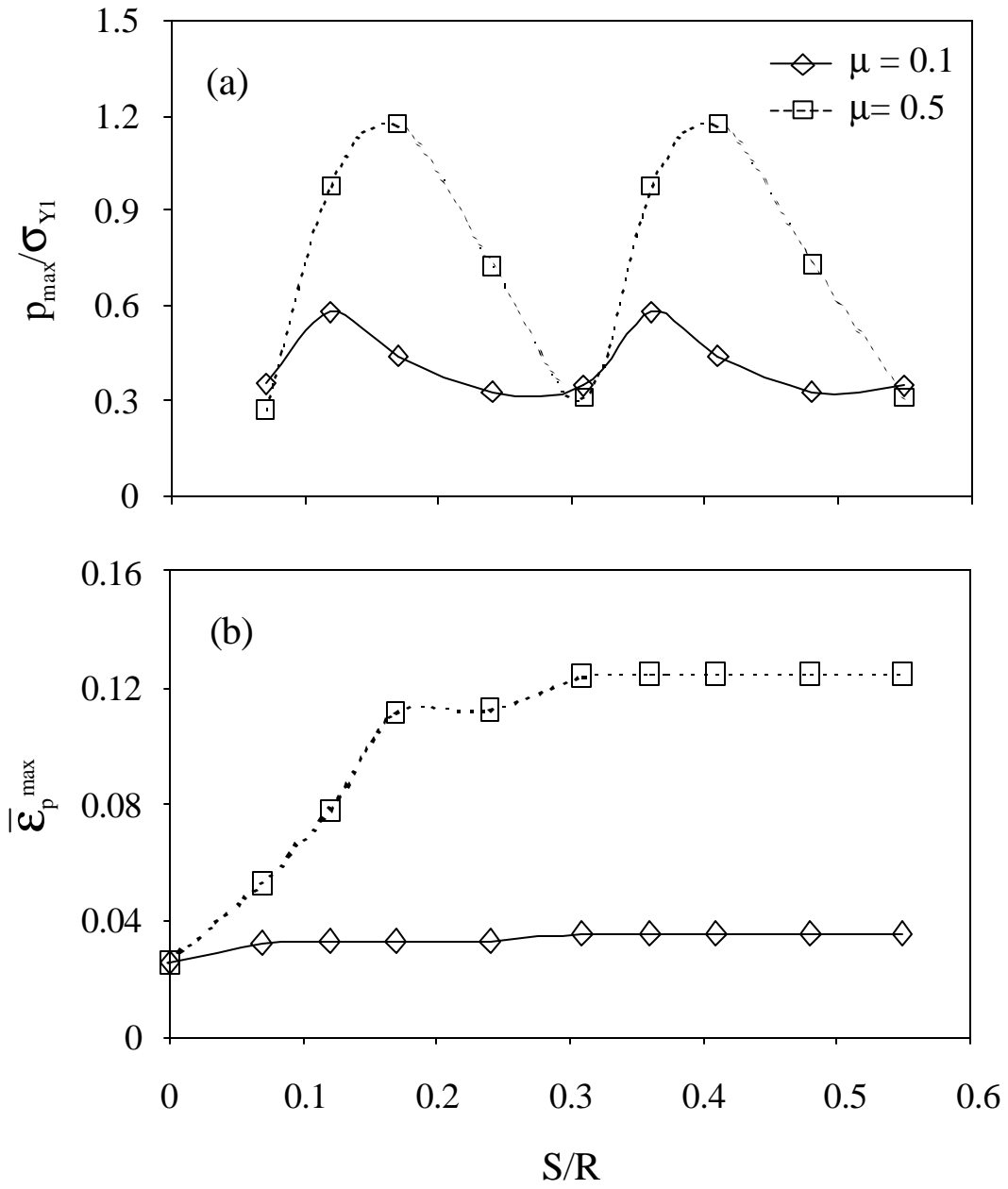


Figure 4

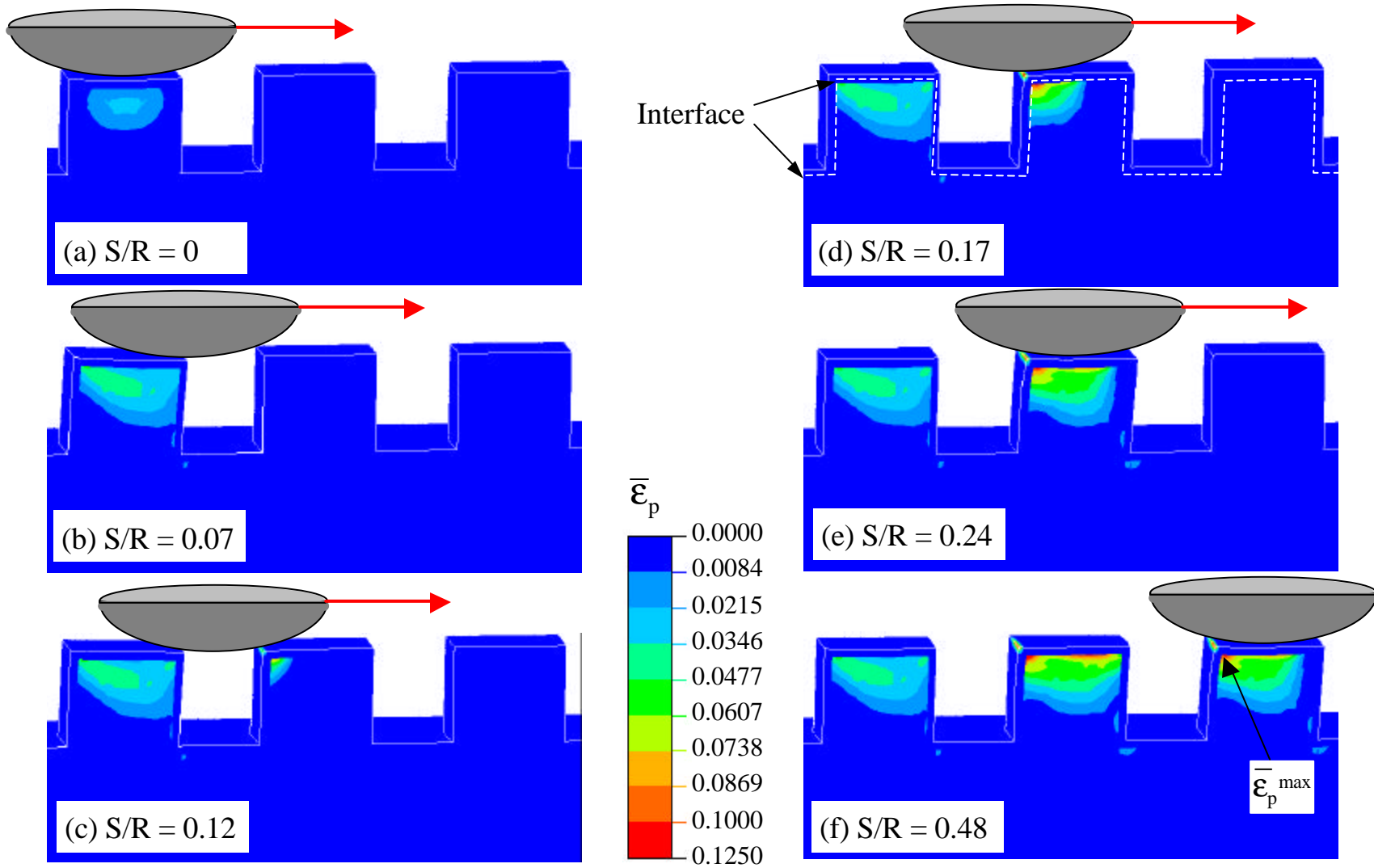


Figure 5

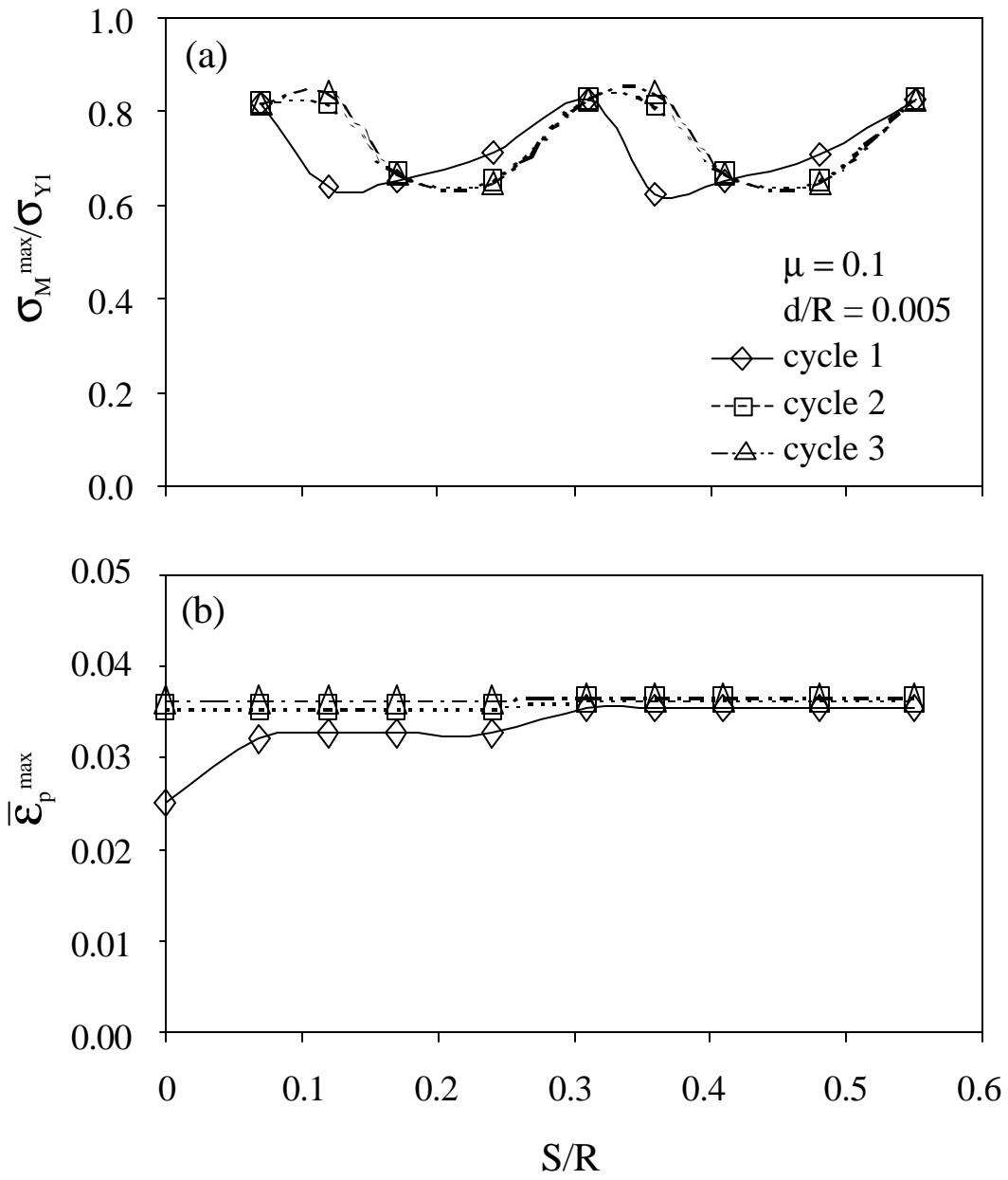


Figure 6

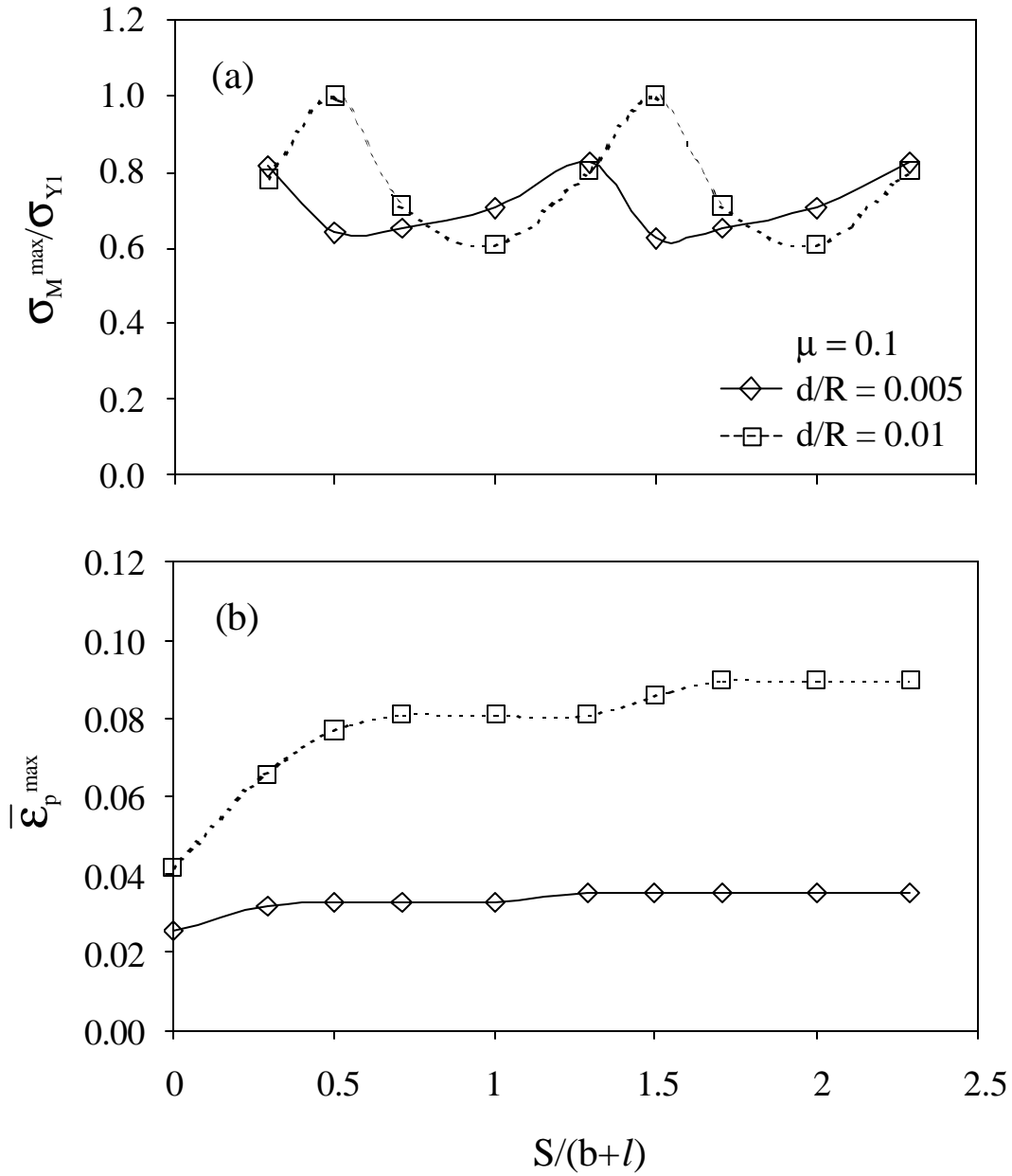


Figure 7

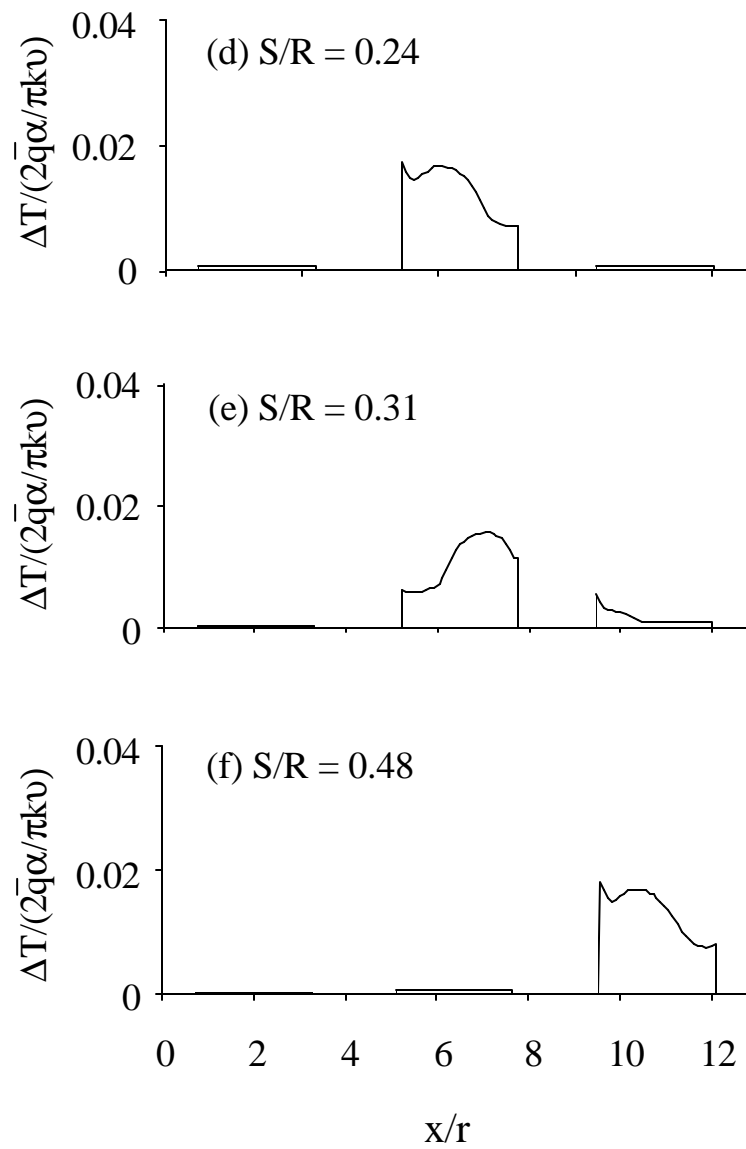
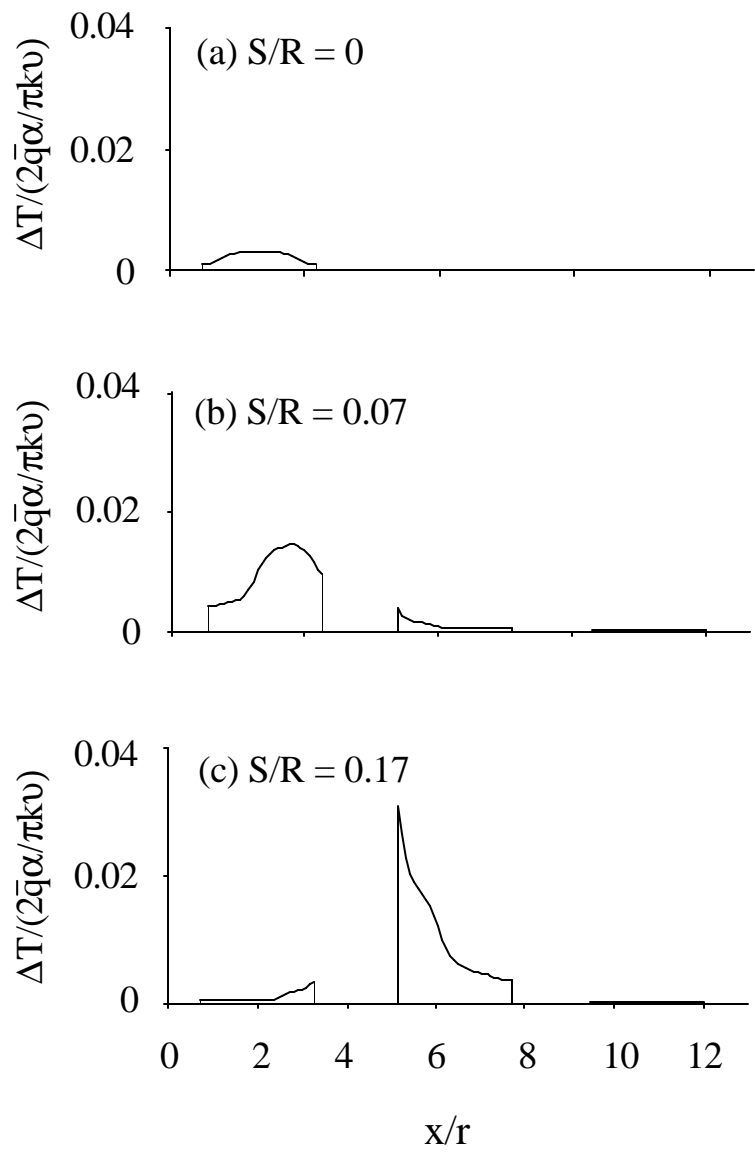


Figure 8

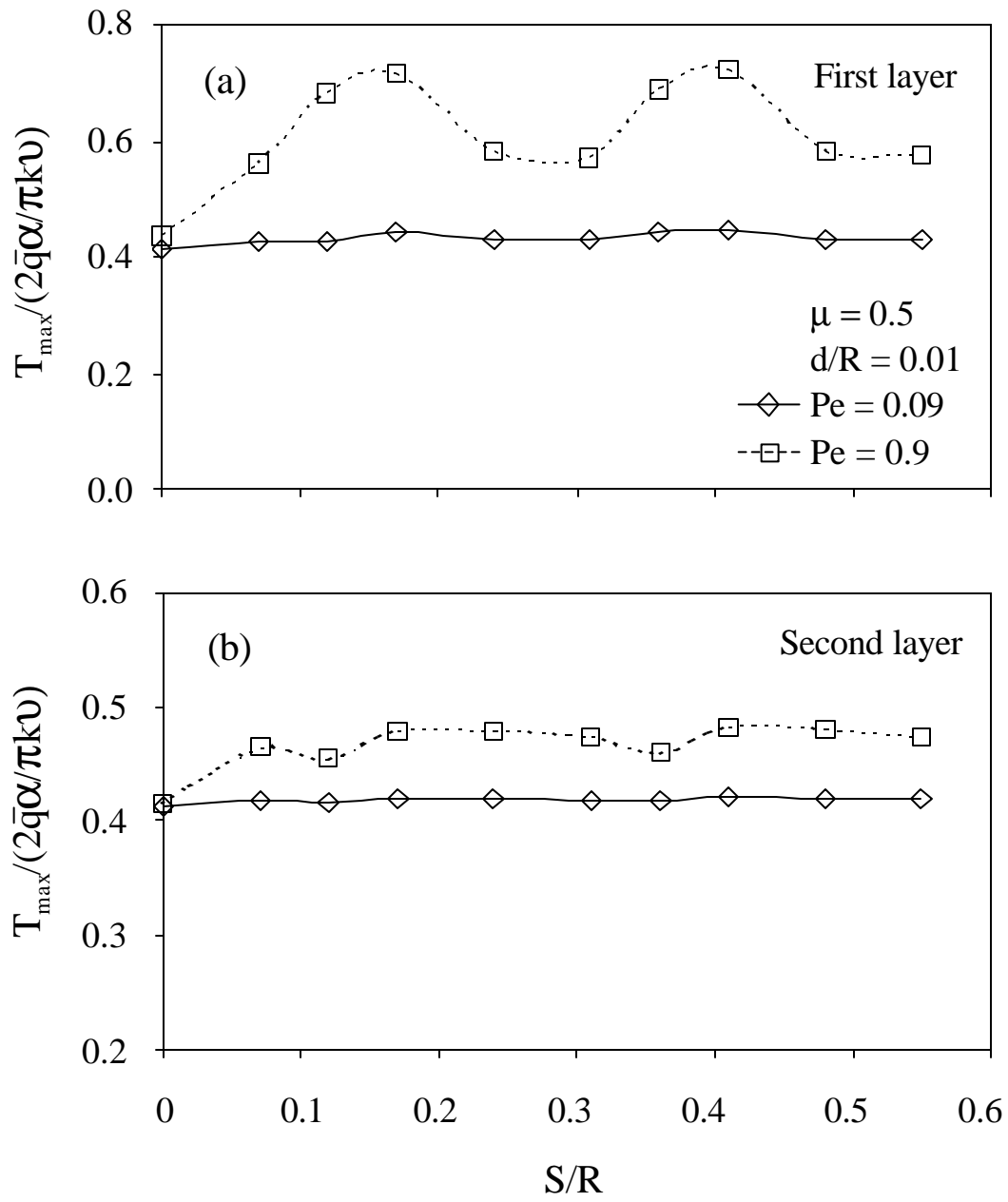


Figure 9

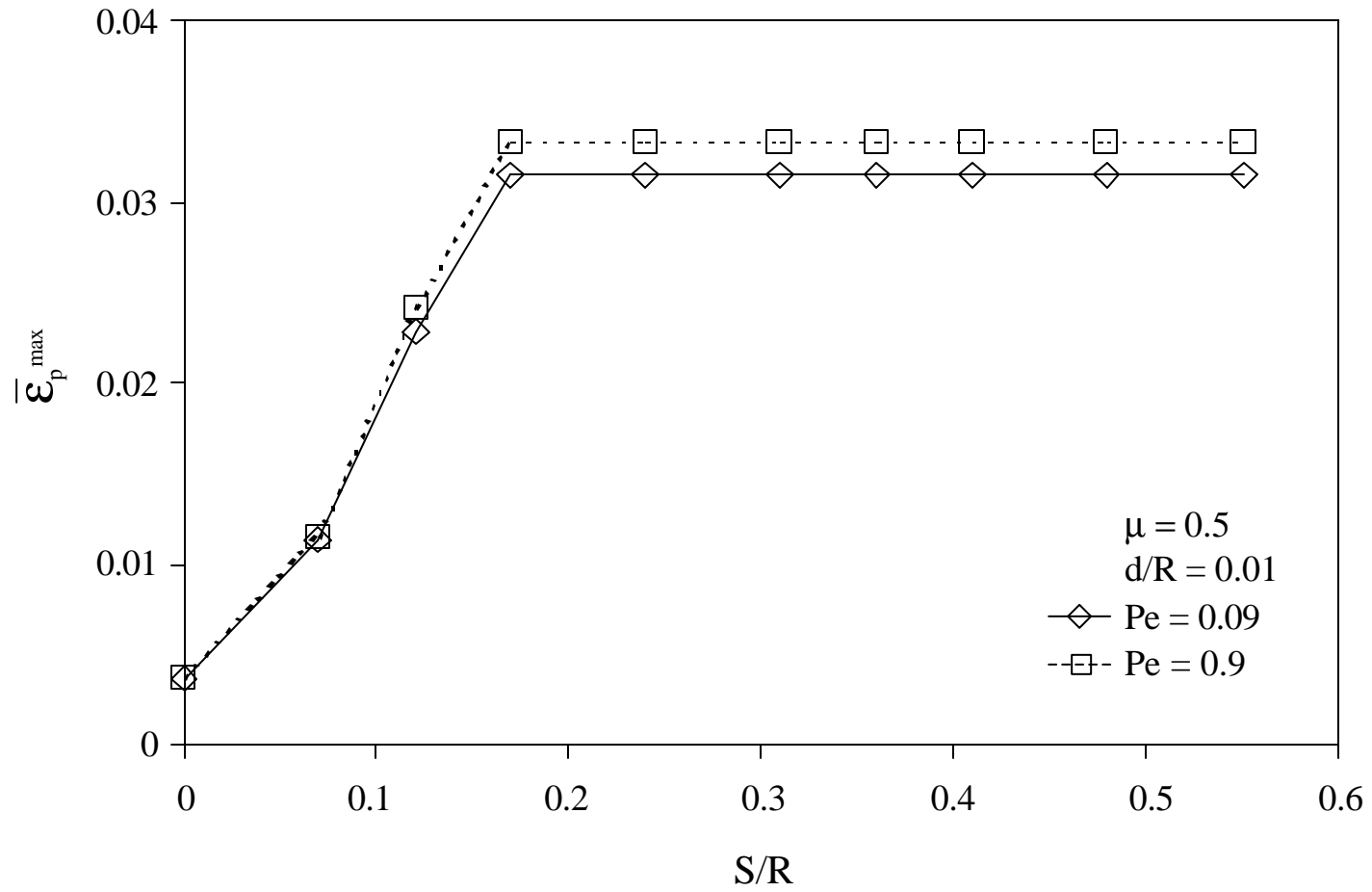


Figure 10